Caustics by reflection and their application to elastic-plastic and dynamic fracture mechanics

Ares J. Rosakis
California Institute of Technology
Graduate Aeronautical Laboratories
Pasadena, California 91125

Alan T. Zehnder
Cornell University
Department of Theoretical and Applied Mechanics
Ithaca, New York 14853-1503

Ramaratnam Narasimhan
Indian Institute of Technology
Department of Mechanical Engineering
Powai, Bombay 400076, India

Abstract. Applications of the method of reflected caustics to the measurement of the J integral in ductile materials are reviewed. It is demonstrated, both numerically and experimentally, that the conditions for accurate interpretation of caustics on the basis of plane stress small scale yielding analyses are often overrestrictive. To overcome these restrictions, we used a three-dimensional, elastic-plastic finite-element calculation to analyze caustics formed by reflection of light from a particular test specimen. Experimental measurements on the same specimen confirm the numerically obtained results. The out-of-plane surface displacements, measured experimentally by interferometry, are in excellent agreement with the corresponding numerical results. In addition, the experimentally obtained caustics agree well with the numerically generated caustics. The excellent agreement between experiment and calculations demonstrates the accuracy of the numerical model and establishes confidence in the interpretation of caustics in the presence of both extensive plasticity and three dimensionality. The analysis of caustics as based on the three-dimensional calculation is applied to the direct optical measurement of the time history of the J integral in a dynamically loaded specimen. The specimen was loaded in a drop weight tower, and the caustics were photographed with a high speed camera.

Subject terms: photomechanics; elastic-plastic fracture; three-dimensional finite elements; caustics by reflection; interferometry; dynamic measurement of J.

Optical Engineering 27(8), 596-610 (August 1988).

CONTENTS

Invited Paper PH-104 received June 10, 1987; accepted for publication May 26, 1988; received by Managing Editor May 31, 1988. This paper is a revision of Paper 814-84, presented at the SPIE International Conference on Photomechanics and Speckle Metrology, Aug. 17–20, 1987, San Diego, Calif. The paper presented there appears (unrefereed) in SPIE Proceedings Vol. 814, Part Two.

1. INTRODUCTION

In recent years the optical method of caustics has been developed into a successful experimental tool for studying linear elastic fracture mechanics problems. In such problems, caustics have been used for the direct optical measurement of stress intensity factors.[1,2] Particularly important applications of caustics have been made in dynamic fracture mechanics, where the stress intensity factor cannot generally be determined analytically.[3,4] The past success of caustics has led to efforts to extend the method to applications in elastic-plastic fracture.

Some preliminary work[5,6] based on the assumption of the validity of the plane stress Hutchinson-Rice-Rosengren (HRR) asymptotic crack tip field[7,8] demonstrated that the value of the J integral can be directly measured with caustics. Unfortunately, the region of dominance of the plane stress HRR field has not been accurately established. Thus, the conditions under which the analytical results reported in Refs. 5 and 6 are valid are uncertain. Nevertheless, experimental results given in Refs. 9 through 12 indicate that the method is promising and is worthy of further investigation.

In this paper we review the limitations in the interpretation of caustics on the basis of plane stress small scale yielding analyses. To overcome such limitations, we use a detailed three-dimensional elastic-plastic finite-element calculation to

simulate a three point bend laboratory specimen. We also use this calculation to construct "synthetic" caustic patterns for different load levels ranging from small scale to large scale yielding conditions.

The numerical calculation is followed by a series of experiments based on caustics and on Twyman-Green interferometry performed simultaneously on both sides of the three point bend specimen. The out-of-plane surface displacements, recorded by interferometry, are compared with the numerically generated near-tip out-of-plane displacements to indicate the accuracy of the three-dimensional numerical model. The caustics experiments are used to obtain the relationship between the caustic diameter D and the value of the J integral for different load levels. This is found to agree well with the equivalent relation between D and J, obtained on the basis of the "synthetic" caustic patterns generated by the numerical solution.

Once complete agreement between theory and experiment is demonstrated, the relation between D and J is used for the interpretation of caustics obtained in dynamic experiments by means of high speed photography. The dynamic experiment utilizes the same three point specimen geometry described above, loaded in a drop weight tower. The resulting caustic patterns are recorded by means of a rotating mirror high speed camera and provide a time history of J^d up to the point of crack initiation. This measurement is, to our knowledge, the first direct optical measurement of $J^d(t)$ under dynamic conditions. The resulting loading rates are of the order of $\dot{J}^d = 10^3$ N/ms.

2. CAUSTICS BY REFLECTION

2.1. Mapping equations

Consider the flat surface of an opaque plate specimen of uniform thickness h, containing a through crack. In the undeformed state, this surface, assumed to be perfectly reflective, will occupy a region in the x_1,x_2 plane at $x_3 = 0$. When loads are applied on the lateral boundaries of the plate, the resulting change in thickness of the plate specimen is nonuniform, and the equation of the deformed specimen surface will be expressed as

$$x_3 + f(x_1,x_2) = 0 . \tag{1}$$

Consider, further, a family of light rays parallel to the x_3 axis, incident on the reflecting surface [Eq. (1)]. Upon reflection, the light rays will deviate from parallelism (see Fig. 1). If certain geometrical conditions are met by the reflecting surface, the virtual extensions of the reflected rays (dashed lines) will form an envelope that is a three-dimensional surface in space. This surface, called the *caustic surface,* is the locus of points of highest density of rays (maximum luminosity) in the virtual image space. The virtual extensions of the rays are tangent to the caustic surface. The reflected light field is recorded on a camera positioned in front of the specimen. The focal plane of this camera, which we call the *screen* for convenience, is behind the plane $x_3 = 0$ (occupied by the reflector in the undeformed state) and intersects the caustic surface at the plane $x_3 = -z_o$, $z_o \geq 0$. On the screen, a cross section of the caustic surface is observed as a bright curve (the *caustic curve*), bordering a dark region (the *shadow spot*). The resulting optical pattern depends on the nature of the

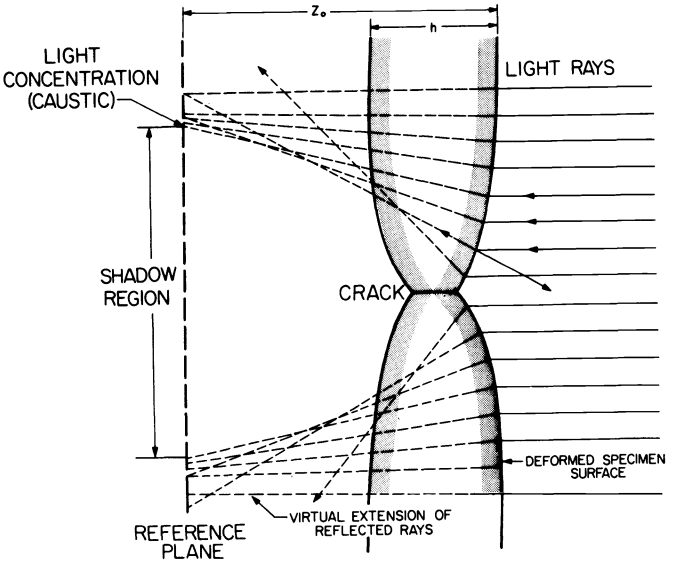

Fig. 1. Formation of caustic due to reflection of light from the polished, deformed specimen surface near a crack tip.

function $f(x_1,x_2)$ and on the focal distance z_o. The reflection process can be viewed as a mapping of points (x_1,x_2) of the plane occupied by the reflector in the undeformed state onto points (X_1,X_2) of the plane $x_3 = -z_o$ (the screen). The mapping equations based on geometrical optics are given by[13]

$$\mathbf{X} = \mathbf{x} - 2(z_o - f)\frac{\nabla f}{1 - |\nabla f|^2} , \tag{2}$$

where $\mathbf{X} = X_\alpha \mathbf{e}_\alpha$, $\mathbf{x} = x_\alpha \mathbf{e}_\alpha$, and $\mathbf{e}_\alpha$ denote unit vectors. In the subsequent discussion Greek subscripts have the range 1, 2 while Latin subscripts take the values 1, 2, and 3.

When $z_o >> f$, as is usually the case in most practical applications, the above simplifies to[13]

$$\mathbf{X} = \mathbf{x} - 2z_o \nabla f . \tag{3}$$

Relation (3) is the mapping equation that will be used in the rest of this discussion.

2.2. Initial curve and its significance

Equation (2), or its approximation Eq. (3), is a mapping of the points on the reflecting surface onto points on the screen. If the screen intersects the caustic surface, the resulting caustic curve on the screen is a locus of points for which the determinant of the Jacobian matrix of mapping Eq. (3) must vanish, or

$$I(x_1,x_2,z_o) = \det[X_{\alpha,\beta}] = \det[\delta_{\alpha,\beta} - 2z_o f_{\alpha,\beta}] = 0 . \tag{4}$$

The above is a necessary and sufficient condition for the existence of a caustic curve. The locus of points on the reference plane $(x_1,x_2,x_3 = 0)$ for which the Jacobian vanishes is called the *initial curve*, Eq. (4). All points on the initial curve map onto the caustic curve. In addition, all points inside and outside this curve map *outside* the caustic.[13] Since the light that forms the caustic curve originates from the initial curve, essential information conveyed by the caustic comes from that curve only.

Equation (4), defining the initial curve, depends parametrically on z_o. Thus, by varying z_o, we may vary the initial

curve position. If z_o is large, the initial curve will be far from the crack tip. If z_o is small, the initial curve will be close to the crack tip. Variation of z_o can easily be achieved experimentally by simply varying the focal plane of the recording camera system. This is an essential property of the method of caustics, and it can be utilized to "scan" the near-tip region to obtain information regarding the nature of the deformation field at different distances from the crack tip. For the case of a crack tip surrounded by a plastic zone, varying z_o will move the initial curve inside or outside the plastic zone, providing information on the nature of the singularity in plastic strains as well as on the character of the surrounding elastic field.

3. INTERPRETATION OF CAUSTICS ON THE BASIS OF PLANE STRESS ANALYSES

The discussion of the previous section, intentionally kept as general as possible, is not restricted by the form of the function $f(x_1,x_2)$ that describes the nature of the deformed specimen surface. In general, $f(x_1,x_2)$ can be identified as the out-of-plane displacement field $u_3(x_1,x_2)$ evaluated on the surface of the plate specimen.

For a cracked plate of uniform thickness and finite, in-plane dimensions, these displacements will, in general, depend on the constitutive law of the material, the applied load, and the details of the specimen geometry (in-plane dimensions and thickness). Given the lack of full-field, three-dimensional analytical solutions in fracture mechanics, such information can be obtained only by means of detailed numerical computations. Such an approach will be taken in Sec. 5.

Nevertheless, there exist certain special cases for which available asymptotic solutions, based on two-dimensional analyses, may provide adequate approximations for the surface out-of-plane displacement field $u_3(x_1,x_2)$. In particular, it can be argued that conditions of generalized plane stress will dominate in thin cracked plates, provided that both the crack length and in-plane dimensions are many times the plate thickness. In such cases, $u_3(x_1,x_2)$ will be approximated by means of available analytical solutions based on plane stress analysis.

3.1. Caustics obtained on the basis of plane stress asymptotic crack tip fields in linear elastostatics

In linear elastic fracture mechanics, the principal application of the method of caustics is to the direct measurement of the mode-I and mode-II stress intensity factors. When a thin cracked plate deforms in a symmetric, mode-I manner, the near-tip out-of-plane displacement field can be approximated by[14]

$$f(r,\theta) = u_3(r,\theta) = \frac{-\nu h K_I}{E\sqrt{2\pi r}} \cos\frac{\theta}{2}, \tag{5}$$

where K_I is the mode-I stress intensity factor, E is the elastic modulus, ν is Poisson's ratio, and h is the specimen thickness. The coordinates r,θ correspond to a polar system centered at the crack tip. Substitution of Eq. (5) into Eq. (3) gives the equations of the optical mapping for this case. The equation for the initial and caustic curves can now be obtained by further imposing the requirement $I = 0$, as expressed by Eq. (4). It is found that the caustic is an epicycloid whose size depends on K_I. In particular, K_I is related to the maximum transverse diameter D of the caustic (width of the caustic in the direction perpendicular to the crack line) by[3]

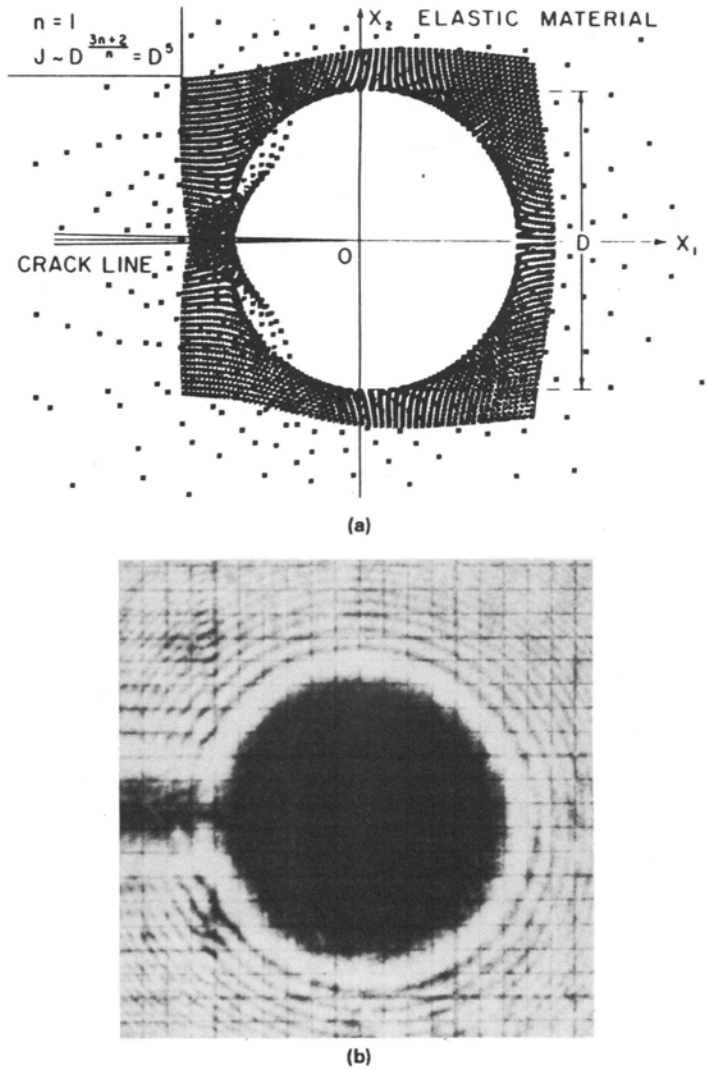

Fig. 2. Caustics formed due to reflection of light from an elastically deforming specimen containing a mode-I crack. (a) Numerically simulated. (b) Experimental.

$$K_I = \frac{ED^{5/2}}{10.7 z_o \nu h}. \tag{6}$$

A caustic constructed analytically using Eqs. (5) and (3) is shown in Fig. 2(a), with a caustic observed experimentally shown in Fig. 2(b). The equation for the initial curve is obtained directly from Eq. (4) and can be shown to be a circle of radius r_o, where

$$r_o = 0.316D = \left[\frac{3h\nu K_I z_o}{2E\sqrt{2\pi}}\right]^{2/5}. \tag{7}$$

It should be observed here that for a given K_I, $r_o \sim z_o^{2/5}$. A variation in z_o, the distance behind the specimen at which the camera is focused, will result in changes in r_o.

It is important to observe that within the framework of linear elastic plane stress analysis, the deformed shape of the specimen surface near the crack tip is known up to a scalar amplitude, which is proportional to K_I. Thus, the light pattern obtained by reflecting parallel incident light from the specimen

surface near the crack tip provides a direct measure of K_I.

Once the method of caustics is described in this way, it becomes clear that the applicability of the method does not hinge on the material in the near-crack-tip region responding in a linear elastic manner. Instead, the key feature is that the deformed shape of the specimen surface in the crack tip region is known up to a scalar amplitude factor. The available asymptotic analyses of crack tip fields in power-law-hardening materials[7,8] suggest that such a situation prevails for these cases as well.

3.2. Caustics obtained on the basis of the asymptotic plane stress HRR field

For stationary cracks and within the framework of small displacement gradients and proportional stress histories, the value of Rice's J integral has been proposed as a plastic strain intensity factor. The viewpoint is adopted here that J provides a suitable scalar amplitude for the deformed shape of the surface of an elastic-plastic fracture specimen at points within the region of dominance of the *plane stress* HRR field.[6] Indeed, for a material whose stress-strain behavior in uniaxial tension may be described by the Ramberg-Osgood model, the near-tip out-of-plane displacement is given by[7]

$$f(r,\theta) = u_3(r,\theta) = -\frac{\sigma_o h}{2E}\left(\frac{JE}{\sigma_o^2 I_n r}\right)^{n/(n+1)}[E_{rr}(\theta,n) + E_{\theta\theta}(\theta,n)] \ , \tag{8}$$

where σ_o is the yield stress in tension, n is the hardening exponent, $E_{rr}, E_{\theta\theta}$ are dimensionless functions of θ on n, and I_n is a scalar function of n, tabulated in Ref. 7.

Substitution of the above equation into Eqs. (3) and (4) provides a relation between D (the maximum transverse diameter of the caustic) and J, which takes the form

$$J = S_n \frac{\sigma_o^2}{E}\left(\frac{E}{\sigma_o z_o h}\right)^{(n+1)/n} D^{(3n+2)/n} \ , \tag{9}$$

where S_n is a scalar function of n, tabulated in Ref. 6. Unlike for the elastic case, the initial curve is no longer circular,[6] and its shape depends on the hardening level of the material. The point (r_o, θ_{max}) on the initial curve that maps onto the maximum value of X_2 of the caustic curve is at an angle θ_{max} measured counterclockwise from the x_1 axis. It is shown in Ref. 11 that θ_{max} varies from 72° to 56° as n varies from 1 to ∞ and that r_o can be related to D by

$$r_o = \begin{cases} 0.385D \ , & n = 9 \ , \\ 0.40D \ , & n \to \infty \ . \end{cases} \tag{10}$$

The caustic pattern for a hardening exponent of n = 9 is shown in Fig. 3. Figure 3(a) shows a caustic predicted from the above analysis, and Fig. 3(b) shows an experimentally obtained caustic. The plastic zone can be seen surrounding the caustic of Fig. 3(b), demonstrating that the caustic is generated from points well within this zone, or equivalently, that $r_o \ll r_p$, where r_p is the plastic zone size at $\theta = 0$. We note that Eqs. (5) through (10) are obtained under the assumption of the validity of particular asymptotic plane stress fields. In the next section we attempt to eliminate this restriction by constructing caustics based on a full-field plane stress numerical solution.

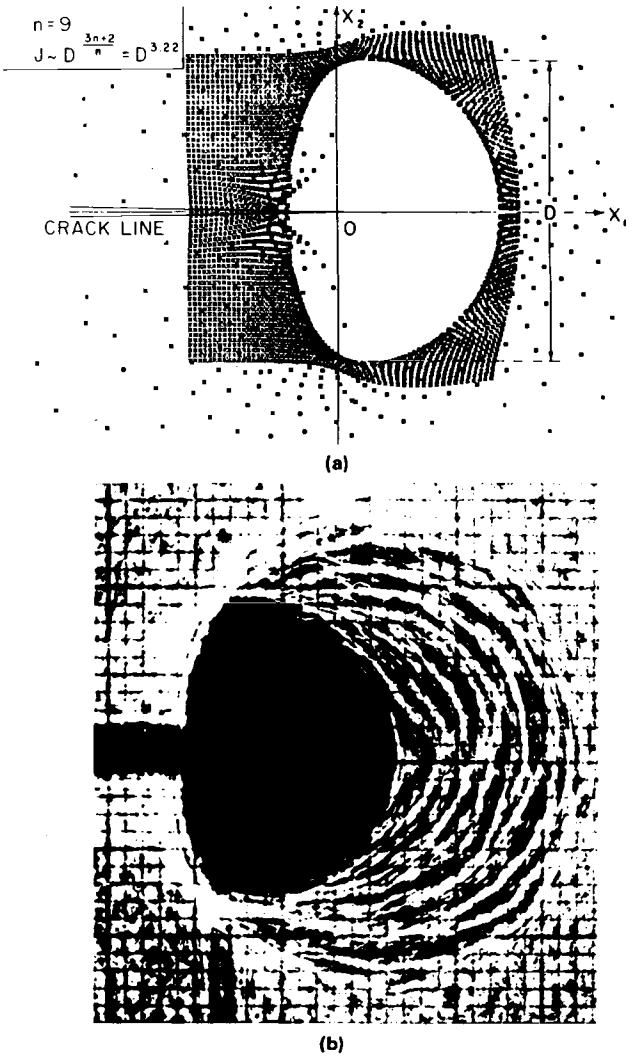

Fig. 3. Caustics formed due to reflection of light from within a crack tip plastic zone. (a) Numerically simulated on the basis of plane stress HRR. (b) Experimental.

3.3. Caustics obtained on the basis of an elastic-plastic plane stress small scale yielding finite-element calculation

The numerical calculations modeled a semi-infinite crack under mode-I plane stress small scale yielding conditions. The details of these calculations are found in Refs. 15 and 16. The displacements of the singular, elastic crack tip field, $\mathbf{u} = K_I(r/2\pi)^{1/2}\hat{\mathbf{u}}(\theta)$, were specified on a circular radius of approximately 3400 times the smallest element, as shown in Fig. 4. The maximum extent of the plastic zone was contained within 1/30 of this radius, ensuring small scale yielding conditions. The cutout in Fig. 4(a) is a fine mesh region around the crack tip, which is shown in detail in Fig. 4(b). An incremental J_2 plasticity theory was used. The material obeyed the Hüber-von Mises yield criterion and followed a piecewise power-hardening law in uniaxial tension of the form

$$\frac{\varepsilon}{\varepsilon_o} = \begin{cases} \dfrac{\sigma}{\sigma_o}, & \sigma \le \sigma_o \ , \\ \left(\dfrac{\sigma}{\sigma_o}\right)^n, & \sigma > \sigma_o \ , \end{cases} \tag{11}$$

with hardening exponents n = 5,9,∞. Here we concentrate on the results for n = 9 since this matches the 4340 steel used in experiments to be described later. All plasticity was confined to the "active region" [Fig. 4(a)], consisting of 1704 four-noded isoparametric quadrilaterals. After the element nearest the crack tip has yielded, the load, applied through the stress intensity factor K_I, or equivalently through J ($J = K_I^2/E$ for small scale yielding), was increased monotonically until the extent of the plastic zone ahead of the crack tip was 50 times the smallest element size. For the propagation phase of this study we used a nodal release procedure[16] to grow the crack by 20 elements. A number of crack growth histories were studied corresponding to different values of Paris's tearing modulus $T = (E/\sigma_o^2)(dJ/da)$ of 0, 1, 5, 15, 20.[16] In the next section we summarize some of the results of the numerical analysis pertaining to the synthetic construction of caustic curves.

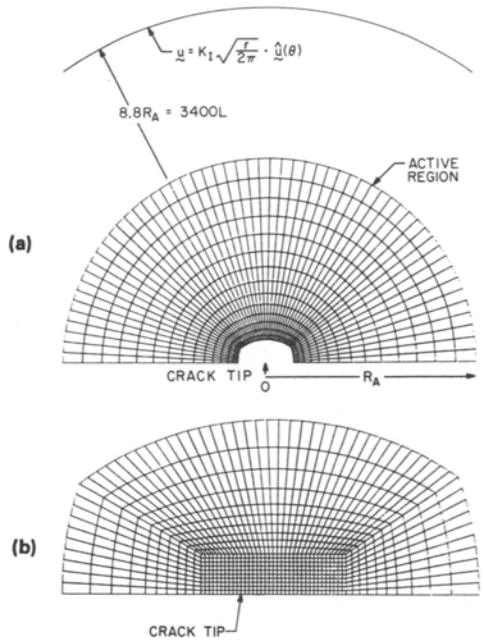

Fig. 4. (a) Finite-element mesh for the 2-D numerical model. (b) Detail of mesh near the crack tip.

3.3.1. *Stationary cracks*

The maximum radial extent r_p of the numerically obtained plastic zone was in good agreement with experimental measurements performed on thin compact tension specimens of 4340 steel, restricted to small scale yielding conditions.[10] The value of r_p was found to be $0.25(K_I/\sigma_o)^2$. Direct comparison of the full-field-stress and deformation fields with their asymptotic, HRR counterparts revealed good agreement for $x_1 < 0.3r_p$, thus establishing the range of dominance of the asymptotic solution. On the other hand, the numerically obtained field quantities were shown to approach the elastic K_I field only well outside the plastic zone, i.e., for $x_1 > 1.5r_p$. If the initial curve satisfies the first of these restrictions, it can be expected that caustics can be interpreted on the basis of Eq. (9). On the other hand, if the second restriction is satisfied, the elastic analysis of caustics is sufficient and Eq. (6) can be used for the evaluation of K_I.

To provide a means of analyzing caustics that is not dependent on the assumption of dominance of either the HRR or K_I fields, caustic patterns were generated using the results of the finite-element analysis. The out-of-plane surface displacements were smoothed using a least squares scheme, and

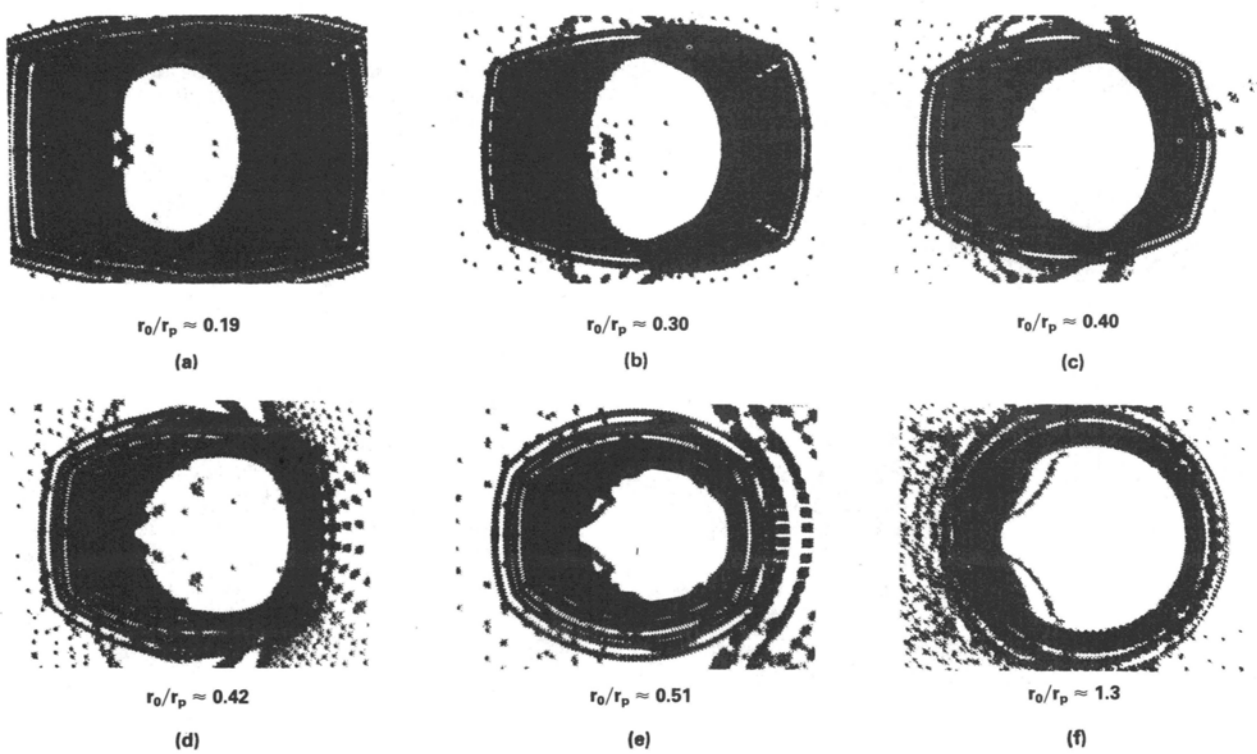

Fig. 5. Caustics generated by using the out-of-plane displacements calculated from the 2-D, small scale yielding numerical model.

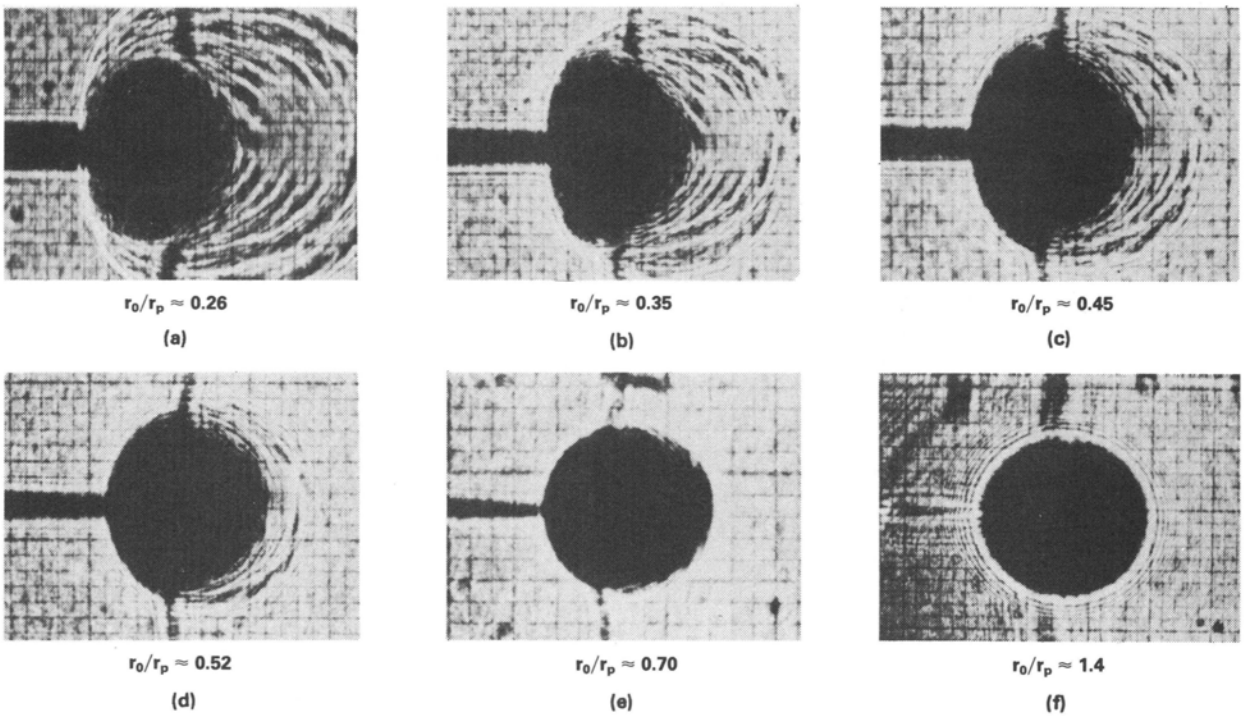

Fig. 6. Sequence of caustics obtained for reflection of light from regions near a plastically deforming crack tip, under small scale yielding conditions.

caustics were generated by mapping light rays point by point using Eq. (3). For a fixed value of applied load (far-field K_I level) a series of caustics was generated corresponding to different values of z_o. As discussed in detail in Sec. 2.2, variation in z_o results in initial curves of different sizes and allows for the complete scanning of the near-tip region. The caustics are shown in Fig. 5 for values of r_o/r_p ranging from 0.19 to 1.3. It is seen that for $r_o/r_p = 0.19$, the numerically simulated caustic agrees in shape with the caustic predicted using the HRR field, Fig. 3. On the other extreme, when $r_o/r_p = 1.3$, the numerically simulated caustic, Fig. 5(f), exhibits the epicycloidal shape of the caustic obtained using the elastic K_I field (see Fig. 2). In the region between $r_o/r_p = 0.19$ and 1.3 there is a transition from the "HRR-like" caustic to the "elastic" caustic.

Figure 6 is a sequence of photographs of caustics obtained from the tensile loading of a thin compact tension specimen of 4340 carbon steel. The experimental details, specimen dimensions, etc. are described by Zehnder, Rosakis, and Narasimhan in Ref. 10. On comparing Figs. 5 and 6, it is seen that in both cases there is a transition from an HRR caustic to an elastic caustic as r_o/r_p goes from 0.19 to 1.3. The transition away from the HRR caustic appears to take place slightly sooner in the numerical model than in the experimental results. However, the general trend is similar in both cases. It is found that both the numerical and experimental caustics retain the shape predicted by the $r^{-1/2}$ field even for r_o/r_p as small as 1.0 Thus, the effect of the plastic zone on the caustic measurement cannot be judged by mere observation of the caustic shape. The reason for the invariance in shape is explained in detail in Ref. 10. The effect of plasticity on the interpretation of caustics obtained when the initial curve lies outside the plastic zone is discussed in Sec. 4.

The numerically generated caustics were also used to establish the relationship between the caustic diameter D and the

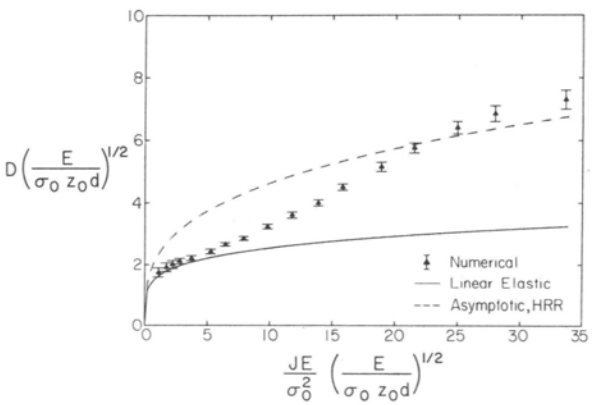

Fig. 7. Relationship between caustic diameter and the J integral for 2-D analyses.

value of applied J for the two-dimensional, small scale yielding problem. This relationship is shown in Fig. 7 in a non-dimensional form. A very small abscissa value in this figure (large z_o or small J) implies that the initial curve is far away from the tip. A large abscissa value implies that the curve is very near the tip, probably within the range of dominance of the HRR field. The solid line in the figure represents the variation of caustic size in the K_I-dominated region, as given by Eq. (6) with $\nu = 0.3$. The dashed line gives the relationship for caustics generated from the HRR-dominated region, as given by Eq. (9). As can be observed from this figure, the full-field numerical results approach the elastic relation (6) for small abscissa values and the relation (9) obtained from the HRR solution for large values of the abscissa. In the intermediate region there is a transition from one relation to the other. The error bars in the figure indicate the uncertainty in the caustic diameter due to the finite-element discretization.

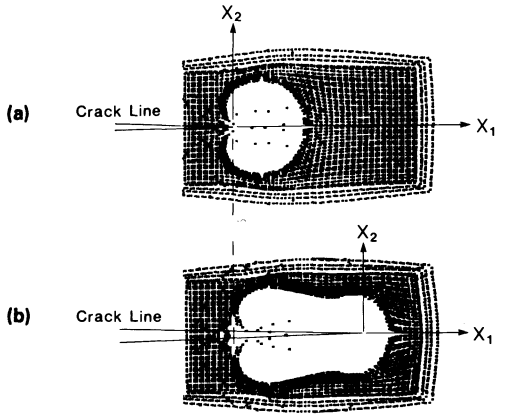

Fig. 8. Numerical caustics from plane stress elastic-plastic analysis. Caustic (a) before crack growth and (b) after crack growth.

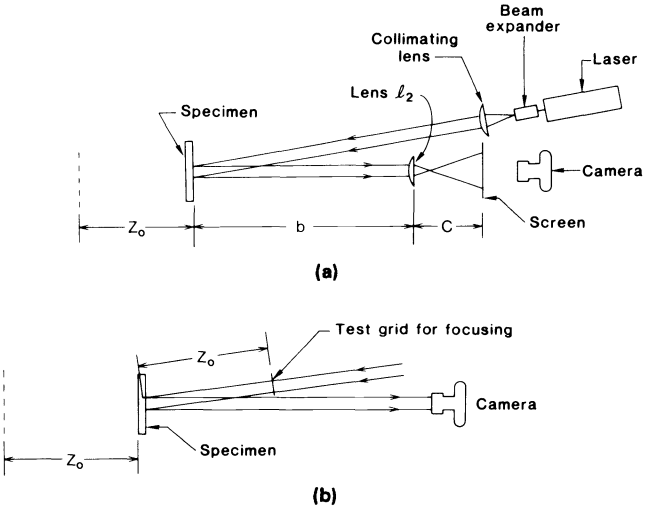

Fig. 9. Optical setups for experiments using reflected caustics. (a) Setup for experiments in which z_o is varied. (b) Setup for fixed z_o.

3.3.2. Growing cracks

The numerical calculations were also used to simulate slow crack growth under plane stress conditions. The details concerning the stress and deformation fields of growing cracks are presented in Ref. 16. For the specific case of an elastic-plastic power-hardening solid with a hardening exponent n = 9, the calculated out-of-plane displacements are used to construct caustics for the initial phases of crack growth. An example of the resulting caustic shapes is shown in Fig. 8. Figure 8(a) displays a caustic corresponding to an initial curve well within the crack tip plastic zone of a stationary crack ($r_o/r_p \sim 0.1$). As expected, the caustic shape is similar to the one calculated on the basis of the HRR analysis.

Figure 8(b) displays the caustic corresponding to an increment of crack length equal to 2/5 of the initial plastic zone size. During crack growth, the value of applied J was kept constant, or $T \equiv (E/\sigma_o^2)(dJ/da) = 0$. It is interesting to observe that the diameter of the caustic curve surrounding the new location of the crack tip is smaller than that of the stationary crack of Fig. 8(a) even though the value of the far-field J was kept constant. This is consistent with the existence of a strain singularity at the tip of a propagating crack that is weaker than that for a stationary crack, as discussed in detail by Narasimhan et al. (see Fig. 2 of Ref. 16). As the crack propagates, there is residual plastic deformation surrounding the initial location of the crack tip and a wake of plastic strains along the newly created fracture surfaces. These plastic strains and the resulting residual out-of-plane displacements are responsible for the residual caustic seen behind the propagating crack tip in Fig. 8(b).

4. EXPERIMENTS USING CAUSTICS

In the previous sections the theory and analysis of the method of caustics were described. In this section two different experimental arrangements used in caustics experiments are discussed, and experiments using caustics in elastic-plastic fracture mechanics are reviewed. The discussion investigates the adequacy of plane stress theories in the interpretation of caustic patterns obtained by reflection of light from the vicinity of through cracks in plate specimens of elastic-plastic materials.

4.1. Description of experiments

Some of the mechanical aspects of setting up an experiment using caustics are discussed here. Two possible optical setups for the recording of reflected caustics are illustrated in Fig. 9. The two setups are identical in principle, but each has distinct advantages for certain types of experimentation. The arrangement of Fig. 9(a) is useful for experiments in which it is desired to photograph caustics corresponding for many z_o values. The arrangement of Fig. 9(b) is useful for experiments in which a fixed z_o value is used and when short exposure times are desired, such as in dynamic fracture experiments.

In both setups a parallel beam of light is reflected from the flat, mirrored surface of the test specimen. The angle between the light beam and the normal to the specimen should be minimized to prevent distortions of the resulting caustics. The light source need not be monochromatic, but it must come from a point source or its equivalent so that the beam can be collimated. The incident beam can be diverging, parallel, or converging; however, a parallel beam is the most useful for many applications.

In Fig. 9(a) the image of the caustic is focused onto a translucent screen by lens ℓ_2. The caustic is then recorded by photographing the screen. The screen can be made of ground glass or even of paper taped to a clear glass or plastic plate. The advantage of this setup is that z_o may be accurately determined by measuring b, c, and the focal length f of lens ℓ_2. Using these values in the thin lens equation, (1/i) + (1/o) = 1/f, one obtains

$$z_o = \frac{cf}{c - f} - b \,. \tag{12}$$

The magnification from the plane at $x_3 = -z_o$ to the real screen is

$$m = \frac{i}{o} = \frac{c}{z_o + b} = \frac{c - f}{f} \,. \tag{13}$$

The measured caustic diameter must be divided by m in the subsequent calculations. To obtain small initial curves, z_o must be small or c large, resulting in high magnification. To obtain large z_o's and large initial curves, c must be small,

resulting in low magnification. To maintain reasonable magnification for large z_o's, a long focal length lens ℓ_2 should be used. The magnification from the screen to the film in the camera is determined by placing a scale on the real screen and photographing the scale superposed on the caustic pattern.

The setup in Fig. 9(b) is commonly applied to dynamic fracture experiments in which a fixed z_o value is used. In this arrangement a test grid, printed on a glass plate, is placed in the incoming beam at a distance z_o from the specimen. The camera is then focused on this grid. The grid may be left in place during the experiment to provide a scale for the photographs of the caustics. In the setup of Fig. 9(a) light is wasted due to the diffuse screen, and thus relatively long exposure times are needed. In the setup of Fig. 9(b) no light is wasted, and with sufficient light very short exposure times are possible. For the dynamic fracture experiments performed at the California Institute of Technology, a 15 ns exposure time is achieved with a 5 W pulsed laser at a 200 kHz pulsing rate.[4]

In photographing caustics one deals only with collimated light and specular reflections. Thus, the camera of Fig. 9(b) must have an aperture large enough to admit the entire light beam and must not obstruct any of the light within the camera. Precise alignment of the camera and the light beam is required. Most commercially available high speed cameras are unsuitable for caustics since they are designed for diffuse light.

4.2. Review of experimental work in elastic-plastic fracture

Very little experimental work has been done to investigate the use of caustics in elastic-plastic fracture mechanics. Preliminary experiments of this sort were reported by Rosakis and Freund.[5] Their work established the feasibility of measuring the J integral with caustics and demonstrated agreement between experimentally observed and analytically predicted caustic shapes.

Further experiments with caustics were performed by Marchand et al.[11] In these experiments the test specimens were of the compact tension type and of varying thicknesses. The loading fixtures allowed for the load and the load point displacement record to be measured. The integration of this record provided an independent measurement of the J integral. The values of J were also obtained from caustics and were interpreted on the basis of the HRR analysis [Eq. (9)]. These were compared with the actual values of J calculated from the load-displacement record. The effect of three dimensionality of the near-crack-tip fields is evident in this work, where it was found that J from caustics is less than the actual J when $r_o/h < 0.5$. Unfortunately, many of the caustics reported in this investigation were very much different in shape from the HRR caustic of Fig. 3. Thus, calculation of J from these caustics by using Eq. (9) based on the HRR field may be inaccurate even if $r_o/h > 0.5$.

A different approach was taken by Judy and Sanford,[12] who performed experiments in which plane stress assumptions were clearly violated. In such cases one cannot hope to use Eq. (9) to determine J from caustics. Instead, the caustic diameter and the J integral were empirically correlated for a number of specimen thicknesses and materials.

Further experiments using caustics for elastic-plastic fracture mechanics were performed by Zehnder et al.[9,10] These experiments investigated the dominance of the HRR fields,

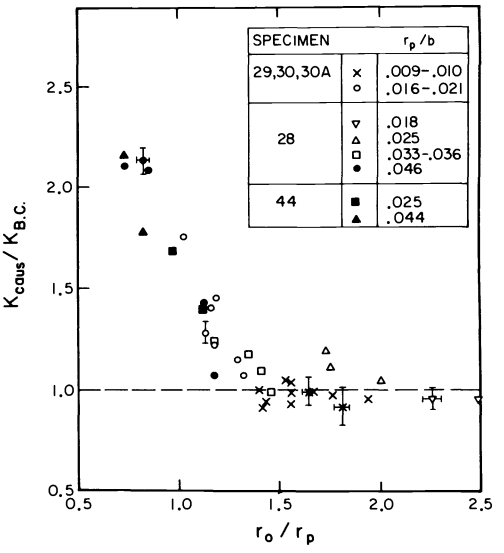

Fig. 10. Error caused by plasticity for caustics generated outside the plastic zone.

the effect of plasticity on caustics originating from the elastic region outside the plastic zone, and the extent of the region of three dimensionality at the vicinity of the crack tip.

The experiments were performed on thin compact tension and three point bend specimens of 4340 and 1018 steel under the restriction of small scale yielding. The J integral (J_{caus}) or the far-field intensity factor (K_{caus}) were measured with caustics using different initial curve sizes. These quantities were simultaneously measured from the boundary conditions and were denoted J_{BC} and K_{BC}. The optical and boundary value measurements were then compared for different loading and specimen configurations. A sequence of caustics obtained from a compact tension specimen at a fixed load is shown in Fig. 6. Only the distance z_o was varied, thus varying the initial curve size r_o. The parameter r_o/r_p in the figure is the ratio of initial curve to plastic zone size. These results were discussed and compared with the numerically generated caustics in Sec. 3.

Under conditions of plane stress small scale yielding, the elastic singular field dominates at some distance outside the plastic zone. Thus, when the initial curve radius r_o satisfies $r_o >> r_p$ and $r_o << a$, where a is the crack length or some other relevant in-plane specimen dimension, K_I may be measured with caustics by applying Eq. (6).

The results of the numerical analysis described in Sec. 3 indicate that the actual stress field deviates from the elastic singular field when $r < 1.5r_p$. Thus, values of K_I as measured with caustics are expected to be influenced by the presence of the plastic zone when $r_o < 1.5r_p$. Experiments were performed to quantify the effect of plasticity on caustics obtained from initial curves outside the plastic zone. The results are presented in Fig. 10, where K_{caus}/K_{BC} is plotted versus r_o/r_p. The results show that far away from the plastic zone Eq. (6) is valid. However for $r_o < 1.5r_p$, K_{caus}/K_{BC} deviates from 1.0, indicating that serious errors will occur if Eq. (6) is applied for the evaluation of caustics in this range.

As was demonstrated by the numerical analysis described in Sec. 3, the plane stress HRR field dominates for $r < 0.3r_p$. Thus, the application of Eq. (9) is restricted to $r_o/r_p < 0.3$ *if* plane stress conditions are satisfied. However, due to the

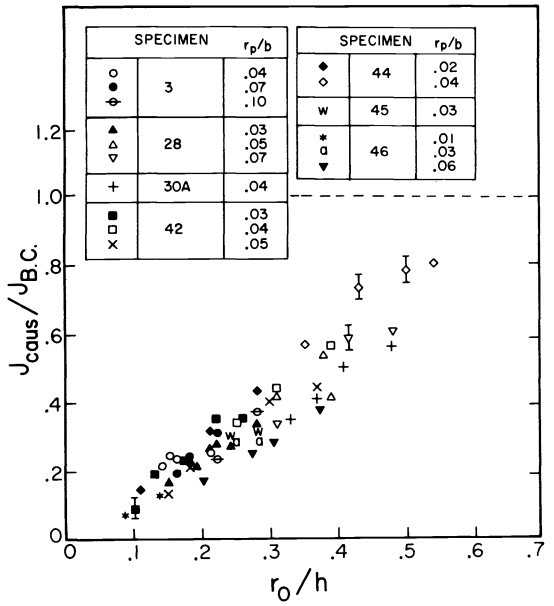

Fig. 11. Error caused by three dimensionality for caustics generated within the plastic zone.

finite thickness of an actual test specimen, there is a region near the crack tip in which the deformation field is three dimensional. Experiments were performed to quantify the effect of three dimensionality on the interpretation of caustics obtained from initial curves that lie within the plastic zone. The results are presented in Fig. 11, where J_{caus}/J_{BC} is plotted versus r_o/h, where h is the specimen thickness. The results show that for $r_o/h < 0.6$, J_{caus}/J_{BC} is less than 1, indicating that three-dimensional effects are important in that region.

As evident from the result of the experiments and the numerical analysis of Sec. 3, the interpretation of caustics on the basis of plane stress small scale yielding assumptions severely limits the applicability of the technique in practical applications. This is most evident near the crack tip, where restrictions on the region of dominance of the plane stress HRR field and the extent of three dimensionality often conflict. Thus, to make caustics useful for studying the toughness of ductile materials, a different approach must be taken. This approach is discussed next.

5. MEASUREMENT OF THE J INTEGRAL WITH CAUSTICS IN THE PRESENCE OF LARGE SCALE YIELDING AND THREE-DIMENSIONAL EFFECTS

As previously discussed, the interpretation of caustics based on either plane stress asymptotic solutions or even numerical plane stress small scale yielding analysis are too restrictive for many practical applications in fracture mechanics. This is because such analyses cannot effectively deal with either three-dimensional effects near the tip or large scale yielding effects, both characteristic of finite test specimen dimensions. In this section, an approach is described that allows for the measurement of the J integral with caustics regardless of specimen dimensions and load level.[17–19] In brief, this approach is a calibration of J versus the caustic diameter D for a particular three-dimensional specimen configuration. This calibration is performed both experimentally and numerically by means of a three-dimensional elastoplastic calculation. The two techniques are compared to establish agreement between the experiment and the numerical calculation. As one might think, a specimen-dependent calibration of this sort has few advantages for static measurements of J when other simpler, more general techniques based on boundary value measurements can be used. On the other hand, such a calibration is very useful for high rate of loading experiments in which one would like to determine the time history of the dynamic value of the J integral, $J^d(t)$, in order to study a material's dynamic fracture toughness. There currently exist no general experimental techniques for making such measurements. The existing techniques[20,21] use measured, dynamic boundary conditions interpreted using quasistatic relations to obtain $J^d(t)$. Because of this interpretation, they are highly restricted in either specimen geometry or loading rate. The only restriction on the method of caustics is that the specimen geometry must be planar and that one must have a high speed camera with a framing rate fast enough to capture a sufficient number of frames during the event.

The investigation described in the following sections is both experimental and numerical. Caustic curves were obtained from a particular specimen configuration at different load levels and were compared with synthetic caustics obtained by finite elements and corresponding to the same load levels. The elastic-plastic finite-element analysis modeled the exact three-dimensional specimen configuration and material constitutive properties. To provide an additional direct comparison between the computation and the actual specimen deformation, a second experiment was performed simultaneously with the caustics experiment. By using Twyman-Green interferometry, the out-of-plane displacement on the specimen surface was measured for load levels up to fracture initiation. These displacements were compared directly with the numerical results. In addition, the load and load point displacement were compared with the numerical results. Further results and details of this investigation are given in Refs. 18 and 19.

5.1. Description of experiments

In this set of experiments,[19] three point bend specimens (number 67 and 69) with a 4:1 length to width ratio were used. The specimen dimensions are given in Fig. 12. The specimens were made of 4340 carbon steel. The heat treatment was 843°C for 1.5 h, oil quench, then anneal for 1 h at 538° C. This resulted in a yield stress σ_o of 1030 MPa and a hardening exponent n of 22.5 for a fit to the piecewise power-hardening law of Eq. (11).

5.1.1. Caustics

The caustics were recorded by means of the setup illustrated in Fig. 13. A wide range of z_o values and load levels was used. The maximum load applied was equal to P_o, the plane stress limit load for the specimen. At low loads (up to 0.7 P_o) the caustic patterns were well defined for all values of z_o. However, when the loads were close to P_o, the caustic curves lost definition for small z_o values. This is because of partial loss of reflectivity of the specimen surface near the crack tip due to extensive plastic deformation. On the basis of this observation we decided to choose a constant value of z_o = 100 cm for subsequent experiments. This choice allowed caustics to be recorded accurately up to the fracture initiation load.

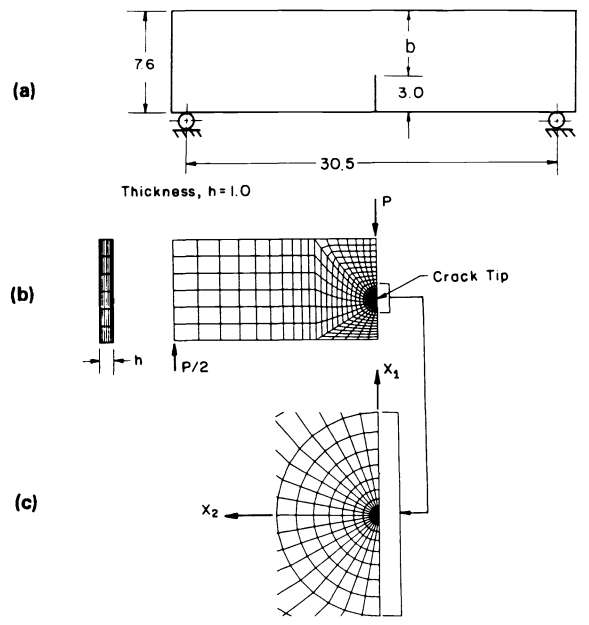

Fig. 12. (a) Test specimen geometry. All dimensions are in centimeters. (b) Mesh for finite-element analysis. (c) Details of the mesh near the crack tip.

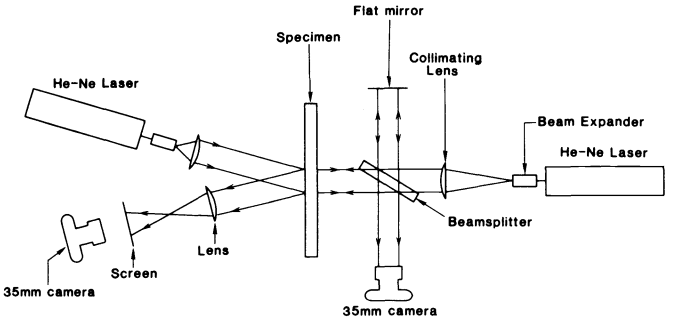

Fig. 13. Optical setup for combined caustics and interferometry experiment.

5.1.2. Interferometry

To provide an additional independent comparison between the numerical calculation and the experiments, a second measurement was performed simultaneously on the other side of the specimen. A version of the Twyman-Green interferometer was used to measure the out-of-plane displacement $u_3(x_1,x_2)$ on the specimen surface. Due to high sensitivity of the interferometric measurement, minimization of vibration of the specimen and optics is important. Thus, the entire apparatus, including the loading frame, was mounted on an isolated optical table. A schematic including both optical arrangements is shown in Fig. 13.

5.2. Numerical analysis

The numerical analysis[18] modeled, in three dimensions, the actual specimen used in the experiments. The geometry of the mesh is shown in Fig. 12(b). It consists of 10 layers of elements through the thickness, each of which is composed of 420 eight-noded brick elements. The layer interfaces are at distances of $x_3/h = 0, \pm 0.15, \pm 0.275, \pm 0.375, \pm 0.45$, and ± 0.5 from the center plane. The details of the in-plane mesh near the crack tip are shown in Fig. 12(c). The smallest in-plane dimension of the element nearest the crack tip is 1/100 the plate thickness.

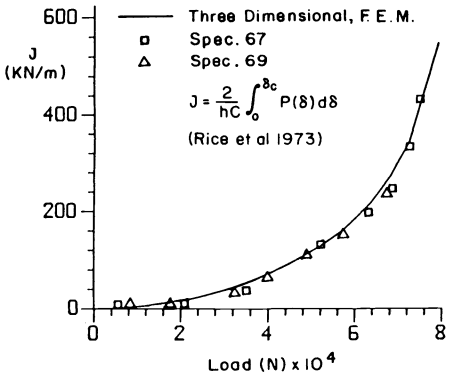

Fig. 14. J integral versus applied load P (experimental and from 3-D numerical analysis).

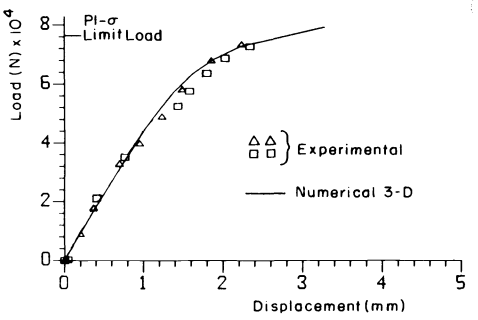

Fig. 15. Load-load point displacement curve.

A small strain, incremental J_2 plasticity theory was used. The material was assumed to be isotropic and to obey the Hüber-von Mises yield criterion. The response of the material in uniaxial tension was characterized by the piecewise power-hardening law of Eq. (11), with a hardening exponent on n = 22 and a yield stress of σ_o = 1030 MPa. These values were chosen to match the constitutive properties of the particular heat treatment of 4340 carbon steel used in the experiments. In the course of the numerical simulation, loads were applied to the specimen incrementally in 140 steps, ranging from 0 to 80,000 N. The average value of the J integral was calculated using a numerical domain integral representation as given in Ref. 22. This average value coincides with the value of J calculated as an integral over a cylindrical surface surrounding the crack front and divided by the specimen thickness. The relationship between J and the applied load is shown in Fig. 14.

5.3. Results: comparison between experiments and calculations

5.3.1. Load displacement record

The first comparison was between the experimentally and numerically obtained load displacement records. The experimental load displacement (P-δ) curves for specimens 67 and 69 are shown in Fig. 15. For each specimen the curve is shown only up to the point of fracture initiation. Also shown is the P-δ curve calculated from the three-dimensional numer-

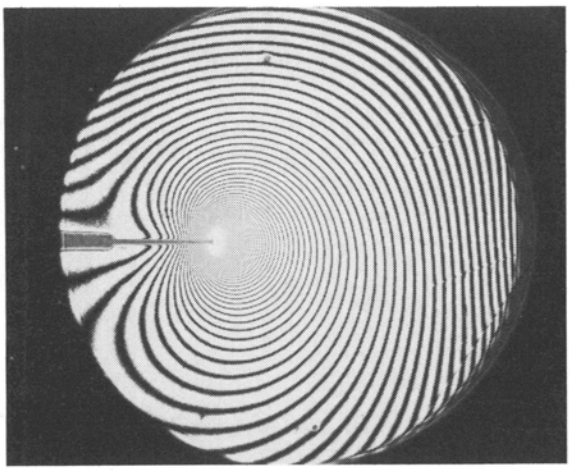

Fig. 16. Interferogram showing crack tip out-of-plane displacements (load: 35,000 N).

ical model. Very good agreement is obtained between the experiments and the calculations.

5.3.2. Interferometry

Since it is displacements that are most accurately calculated in the finite-element method, these were chosen for the most direct comparison with the experiments. The out-of-plane displacements on the specimen surface were measured with interferometry. Interferograms were recorded for load levels ranging from 6000 N up to fracture initiation (74,700 N). At the highest load levels the quality of the interferograms deteriorates. This is due to the roughening of the surface, resulting from plastic deformation near the crack tip, and also to the high fringe density near the crack tip. The highest load for which fringes very near the crack tip could be resolved was 57,300 N.

Typical interferograms are presented in Figs. 16 and 17. Figure 17 shows that fringes can be resolved almost all of the way up to the crack tip (up to three crack opening displacements), except for the part obscured by a small caustic. Each interference fringe represents a line of constant out-of-plane displacement on the specimen surface. Thus, the interferogram is a contour map of the specimen surface.

The numerical contour map on the bottom of Fig. 17 is a synthetic interferogram obtained from the out-of-plane displacements calculated from the three-dimensional numerical model. The displacement increment between lines is the same as in the optical interferogram and is equal to 0.317 μm, or half the wavelength of light. Good agreement is obtained between the experimental and the synthetic interferograms.

A more quantitative comparison beween the experimental and the numerical results is presented in Fig. 18. Here, the experimentally obtained out-of-plane displacement $u_3(r,0)$ along the line $\theta = 0$ is plotted as a function of normalized radial distance r from the crack tip. The displacement is normalized by J/σ_0 and corresponds to a load of 52,000 N. Also shown are the numerical results for the displacements corresponding to the same load level. The extent of the plastic zone ahead of the crack as well as the location along the x_1 axis corresponding to half the specimen thickness are shown for reference. The out-of-plane displacements corresponding to the plane stress HRR field at the same average J value are also plotted for comparison.

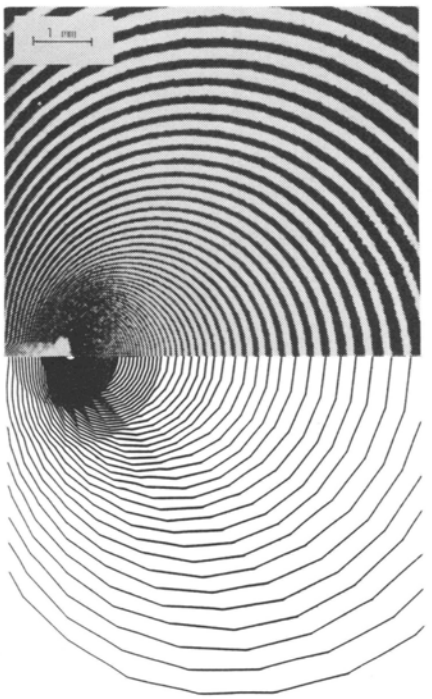

Fig. 17. Comparison between experimental and numerical interferograms. Experimental interferogram corresponds to an enlargement of Fig. 16.

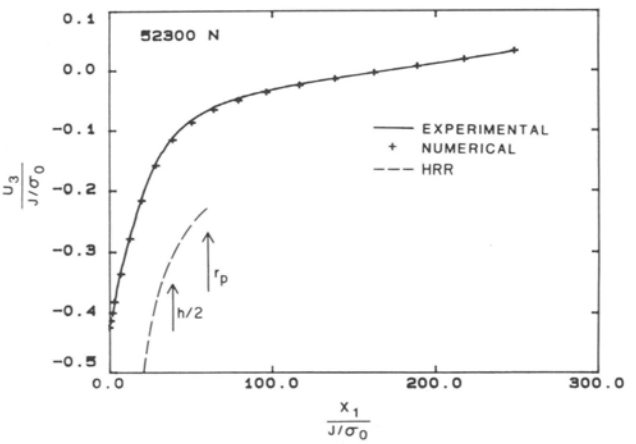

Fig. 18. Nondimensionalized u_3 displacement on the line $\theta = 0$, for 52,300 N load. Comparison between experiment and 3-D numerical analysis.

The first observation is the excellent agreement between the experimental and three-dimensional numerical results. The agreement of the calculated and measured u_3 displacements as well as the agreement of other measured quantities leaves no question that the numerical calculations are sufficiently detailed to model the deformations in the specimen accurately.

For all load levels it was found that there is no region for which the plane stress HRR field adequately described u_3 on the specimen surface. This is consistent with results described in Sec. 4, where it was found that caustics based on the HRR fields could not always be used to accurately measure J. The asymptotic HRR field does not agree with the actual field because of three dimensionality of the near-crack-tip fields

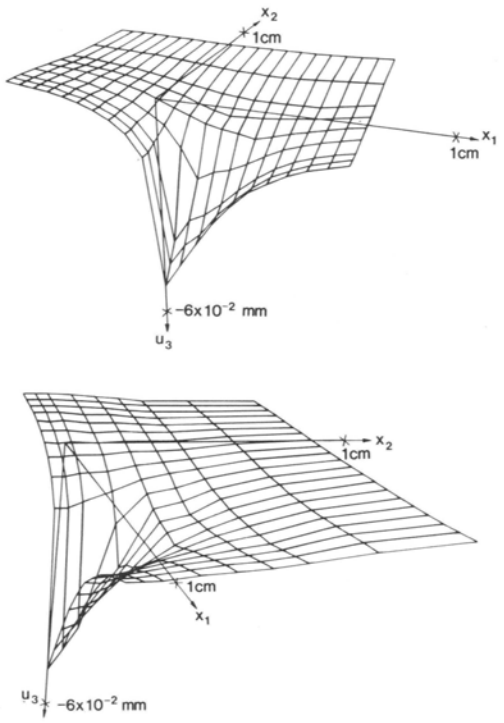

Fig. 19. Alternate views of experimental u_3 displacement for 52,300 N.

and because of the finite specimen dimensions that cause higher order terms to become important away from the crack tip.

To help visualize the nature of the deformed specimen surface, two different views of the experimentally obtained u_3 are plotted three dimensionally in Fig. 19.

5.3.3. Caustics

In the previous section we were able to demonstrate that in terms of out-of-plane displacements, the numerical results are in excellent agreement with experiment. This indicates that it should be possible to generate caustics numerically that agree well with the experimentally observed caustics and are useful for measuring the J integral. In this section this hypothesis is tested.

Caustics are first recorded experimentally for specimens 67 and 69 using a fixed value of z_o = 100 cm. The sequence of caustic patterns for increasing loads up to fracture initiation is shown in Fig. 20. For the same value of z_o and the same loads, caustics are also generated numerically from the results of the 3-D finite-element analysis. These are also displayed in Fig. 20. All of the caustic curves, both experimental and numerical, are reproduced here at the same scale. The values of J shown are obtained through the numerical calculation and are related to the applied load through Fig. 14. The comparison shows that there is good agreement, in shapes and sizes, between the experimental and numerical caustics.

Both experimental and numerical results were used to obtain a relation between caustic diameter D and the J integral, which is shown in Fig. 21 in a nondimensional form. J was obtained from the numerical calculation, while D was measured directly from the experimentally and numerically generated caustics. Also shown in the figure are the J versus

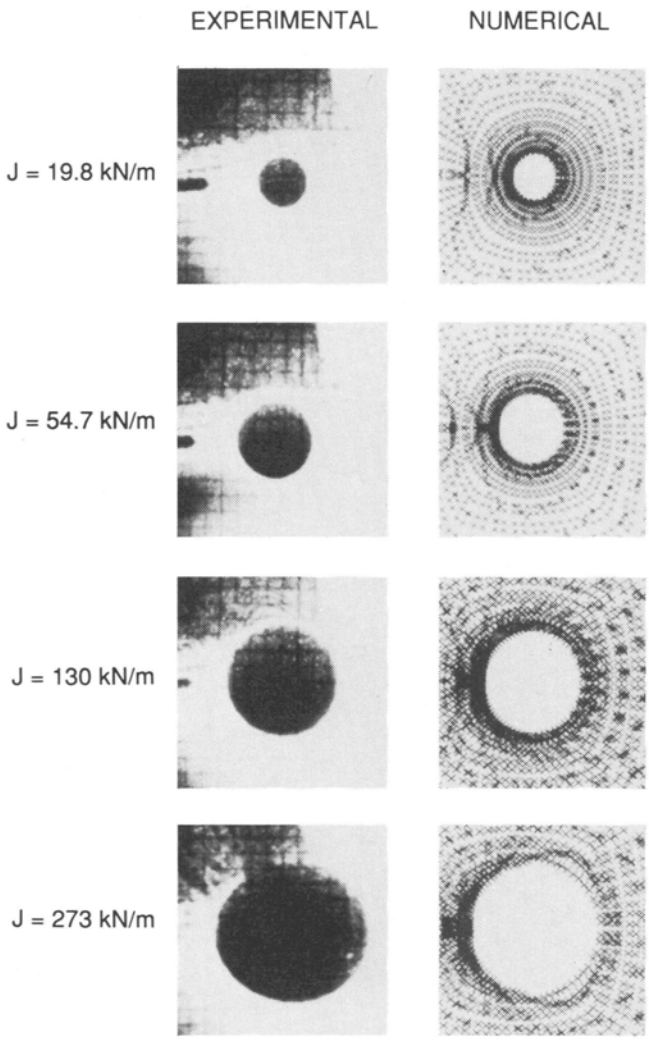

Fig. 20. Sequence of caustics, z_o = 100 cm. Experimental results from specimen 67. Numerical results from 3-D numerical analysis.

D relations obtained on the basis of the plane stress elastic analysis, Eq. (6), and also on the basis of the plane stress HRR field, Eq. (9).

It is seen that the experimental and numerical results are in excellent agreement. This demonstrates that such a calculation can be used to provide an accurate analysis of caustics in the form of a calibration for measuring the J integral. A best fit curve is also shown in Fig. 21. This fit serves here as an empirical relationship between the caustic diameter and the J integral when the relationship based on two-dimensional asymptotic analyses is invalid. This relationship is valid only for the specimen tested here and only for z_o = 100 cm. The relationship will be used in the next section as a master curve for interpreting dynamic fracture experiments on specimens of the same material geometry and with the same z_o.

As was done in the previous two-dimensional numerical analysis, caustics can also be generated for a sequence of z_o values but with a fixed load. Such a sequence is shown in Fig. 22. As before, there is a transition in caustic shape from one that looks like the HRR caustic for small z_o to a more circular caustic at large z_o. Shapewise, these numerically generated caustics agree well with caustics observed experimentally for different z_o's.

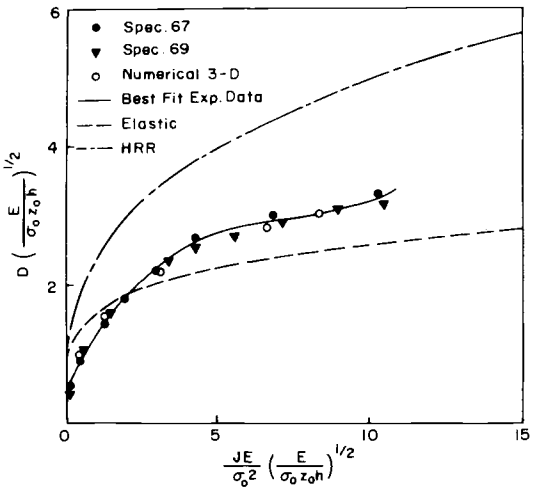

Fig. 21. Relationship between caustic diameter D and J integral. Comparison between experimental and 3-D numerical results.

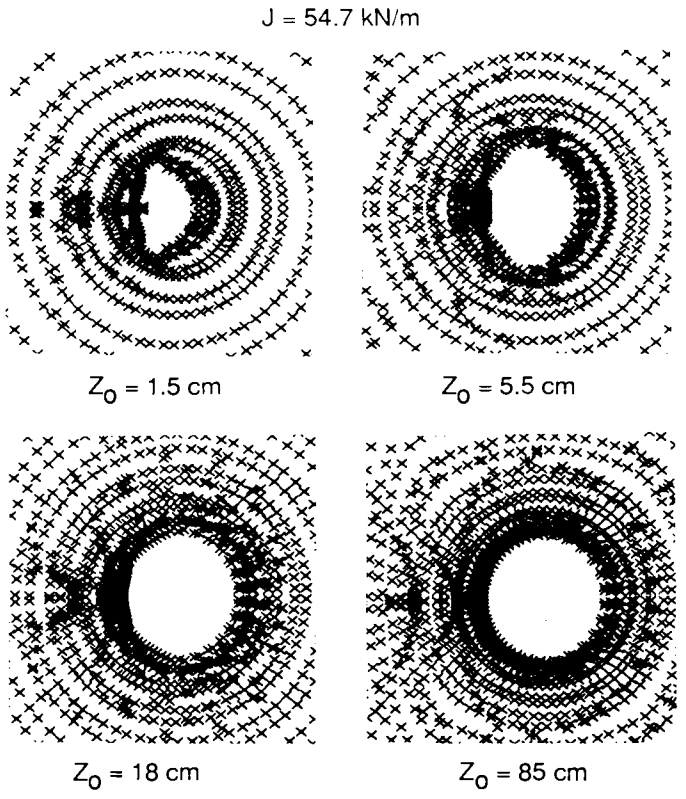

Fig. 22. Sequence of caustics obtained numerically for a fixed load by varying z_0 (from 3-D elastic-plastic analysis).

The excellent agreement here between experiments and calculations demonstrates the accuracy of the numerical model and establishes confidence in the interpretation of caustics in the presence of both extensive plasticity and three-dimensional fields.

6. DYNAMIC OPTICAL MEASUREMENT OF J

In the previous sections we discussed a number of issues related to the use of caustics for the measurement of near-tip parameters in elastic-plastic fracture. The numerical calculations and experiments were performed under quasistatic conditions. Under such circumstances, the use of caustics does not present any particular advantage over other, more established experimental techniques (e.g., compliance techniques). Our major goal in this part is to demonstrate that caustics can be used effectively for the direct (optical) recording of the time history of J^d in a ductile metal specimen subjected to dynamic loading conditions. The results presented here are preliminary and are designed to show the feasibility of measuring $J^d(t)$ with caustics in a dynamic situation. Further developments are described in Ref. 23.

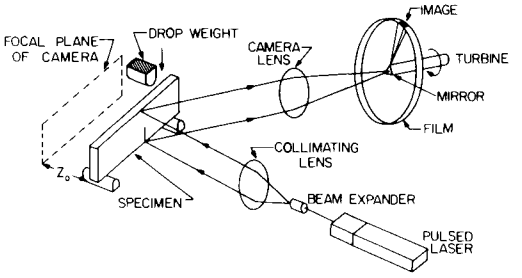

Fig. 23. Setup for dynamic fracture initiation experiments using the method of caustics by reflection.

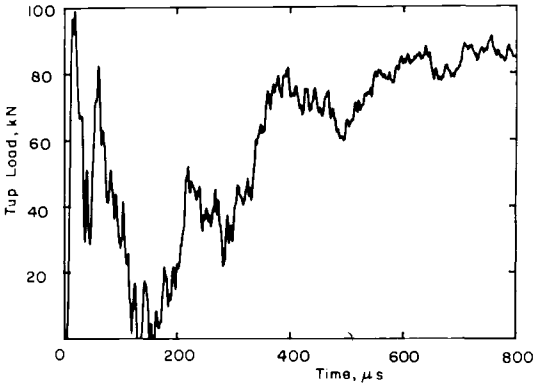

Fig. 24. Tup load record for specimen 71.

6.1. Description of experiments

Three point bend specimens (numbers 70 and 71) of the same dimensions and heat treatment as those in Sec. 5 (see Fig. 12) were tested in a drop weight tower. The experimental setup is sketched in Fig. 23. The drop weight was 1910 N and the impact speed was 5 m/s. Caustics were photographed with Caltech's high speed camera at a rate of 100,000 frames per second. The tup (impactor) and the supports are instrumented with semiconductor strain gauges to allow for the tup load and the support loads to be recorded on a high speed digital oscilloscope. In these experiments interest was confined to recording the J integral up to the time of fracture initiation.

6.2. Results and discussion

The measured tup load (impact load) record for specimen 71 is given in Fig. 24. The load record is highly dynamic, and it is clear that determination of J from the static load versus J results is hopeless for short times. The high speed photo-

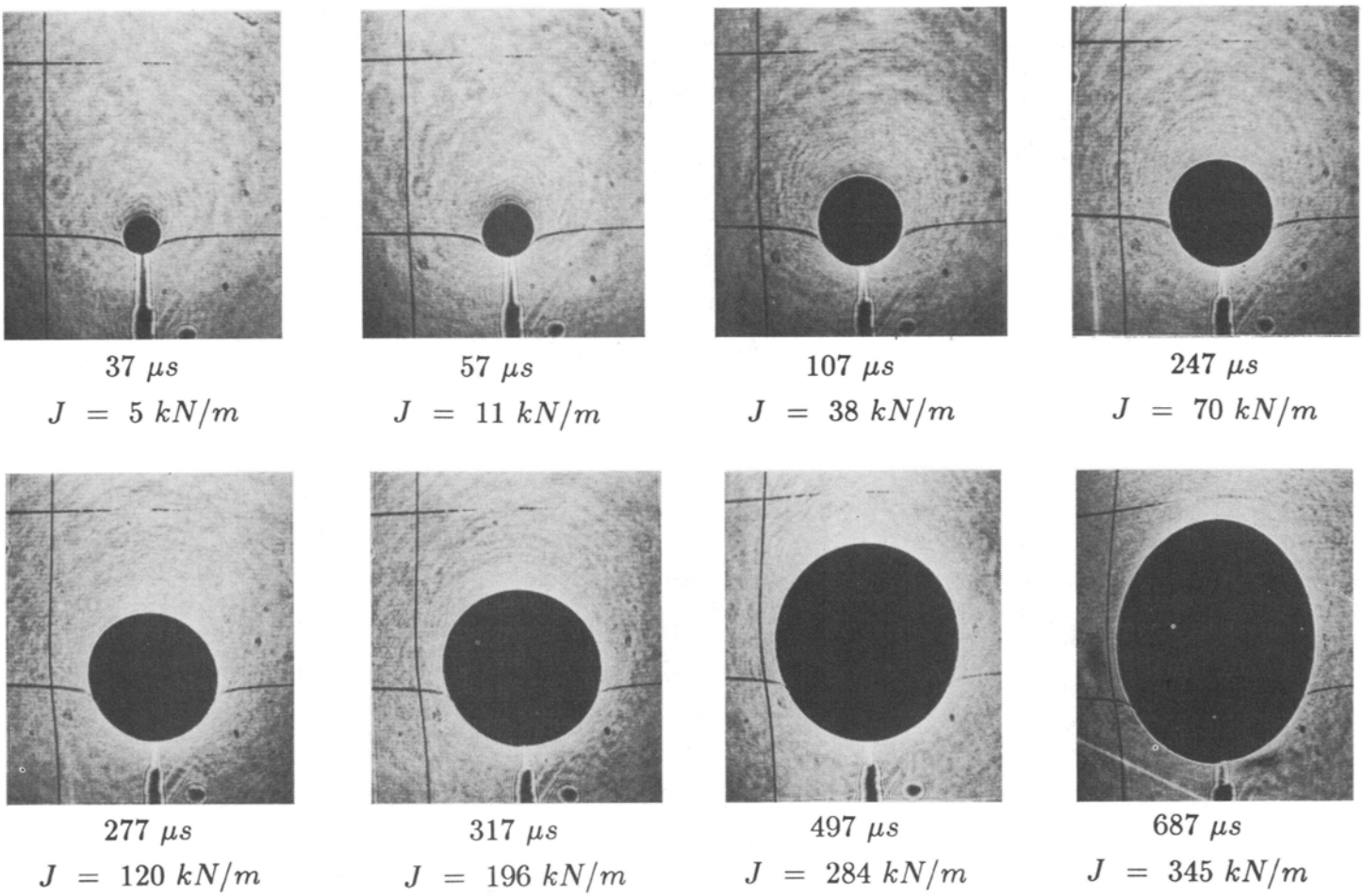

Fig. 25. Dynamic sequence of caustics photographed during drop weight experiment, specimen 71.

graphs indicate that the fracture initiation time was 700 μs. It is seen from Fig. 24 that the tup load showed no decrease at that time. Thus, the load record gives no indication of the time of fracture.

Selected caustics photographs from specimen 71 are shown in Fig. 25. These caustics correspond in size and shape to those recorded statically, Fig. 20. The size and shape of the static and dynamic caustics agree well, except for the last recorded dynamic caustic, which is elongated, indicating crack tunneling.

Crack growth fracture in these thin, ductile specimens occurs in a shearing manner (there is no flat fracture region); thus, when the crack initiates, the caustic becomes asymmetric due to the shearing type of fracture. The appearance of this asymmetry provides the fracture initiation time. The time to fracture was 700 μs for specimen 70 and 780 μs for specimen 71.

Using the static caustics calibration of Fig. 21 and the caustics photographed with the high speed camera, $J^d(t)$ was determined for each specimen and is presented in Fig. 26. The results are given only up to the time of fracture initiation. It is seen that the $J^d(t)$ record contains few of the dynamic oscillations of the tup load.

The reason for performing a fracture initiation experiment under dynamic loading is to investigate the effect of the loading rate on dynamic fracture toughness. Thus, accurate predictions of dynamic fracture initiation require dynamic fracture toughness experiments in initially notched and prefatigued specimens. Although the current experiments were not true fracture toughness measurements since they were not performed with a fatigued crack tip but with a crack of diameter 0.3 mm, it is useful to compare the fracture initiation values J_c from the static and dynamic experiments with the same initial crack tip bluntness. Statically, $J_c \sim 420$ kN/m. Dynamically, $J_c^d \sim 350$ kN/m for both specimens.

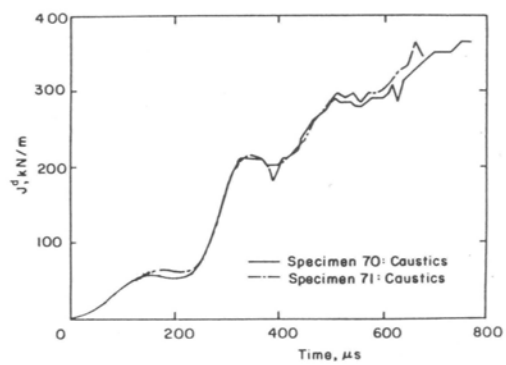

Fig. 26. $J^d(t)$ record from caustics. Results are given for times up to fracture initiation.

6.3. Conclusions

For the first time, the J integral has been measured dynamic-

ally for a ductile material using an optical technique. Although there exist other procedures for measuring J^d in drop weight testing,[20,21] these techniques are most useful for experiments in which the time to fracture is somewhat long and quasistatic approximations of J^d become acceptable. The specimen tested here has a fracture initiation time of 700 μs, which is just borderline on being long enough to apply existing techniques. The interpretation of the optical method of caustics proposed here is not restricted to long fracture initiation times, and thus it complements existing techniques by providing a measurement that can be used for very high loading rates.

We are currently comparing the results of the present experimental technique based on caustics with the results of dynamic numerical calculations performed on the same specimen geometry and subjected to the same transient loading history.[23]

7. ACKNOWLEDGMENTS

This work was supported by the Office of Naval Research through contract N00014-85-K-0596. The computations were performed using the supercomputer at the University of California at San Diego. This was made possible by support from the National Science Foundation through contract MEA-83-07785.

8. REFERENCES

1. P. Manogg, "Anwendungen der Schattenoptik zur Untersuchung des Zerreissvorgangs von Platten," Ph.D. thesis, Freiburg, FRG (1964).
2. P. S. Theocaris and E. Gdoutos, "An optical method for determining opening-mode and edge-sliding-mode stress-intensity factors," J. Appl. Mechan. 39, 91–97 (1972).
3. J. Beinert and J. F. Kalthoff, "Experimental determination of dynamic stress intensity factors by the method of shadow patterns," in *Mechanics of Fracture*, Vol. VII, G. Sih, ed., pp. 281–320, Sijhoff and Noordhoff, (1981).
4. A. T. Zehnder and A. J. Rosakis, "Dynamic fracture initiation and propagation in 4340 steel under impact loading," GALCIT Rept. SM 86-6, Caltech (1986); submitted to Int. J. Fracture (1988).
5. A. J. Rosakis and L. B. Freund, "Optical measurement of the plastic strain concentration at a crack tip in a ductile steel plate," J. Eng. Mater. Technol. 104, 115–120 (1982).
6. A. J. Rosakis, C. C. Ma, and L. B. Freund, "Analysis of the optical shadow spot method for a tensile crack in a power-law hardening material," J. Appl. Mechan. 105, 777–782 (1983).
7. J. W. Hutchinson, "Singular behavior at the end of a tensile crack in a hardening material," J. Mechan. Phys. Solids 165, 13–31 (1968).
8. J. R. Rice and G. F. Rosengren, "Plane strain deformation near a crack tip in a power-law-hardening material," J. Mechan. Phys. Solids 16, 1–12 (1968).
9. A. T. Zehnder and A. J. Rosakis, "A note on the measurement of K and J under small scale yielding conditions using the method of caustics," Int. J. Fracture 30, R43–R48 (1986).
10. A. T. Zehnder, A. J. Rosakis, and R. Narasimhan, "Measurement of the J integral with caustics: an experimental and numerical investigation," GALCIT Rept. SM 86-8, Caltech (1986); to be published in ASTM STP 995 *Nonlinear Fracture Mechanics*, Proc. Third Int. Symposium on Nonlinear Fracture Mechanics (Knoxville, Tenn., Oct. 6–8, 1986).
11. A. Marchand, L. B. Freund, C. C. Ma, and J. Duffy, "Use of the shadow spot method in evaluating J for ductile steels," Brown Univ. Technical Rept. ONR 0597/1, MRL E-160 (1986).
12. R. W. Judy and R. J. Sanford, "Correlation of optical caustic behavior with fracture properties of high strength steels," to be published in ASTM STP 995 *Nonlinear Fracture Mechanics*, Proc. Third Int. Symposium on Nonlinear Fracture Mechanics (Knoxville, Tenn., Oct. 6–8, 1986).
13. A. J. Rosakis and A. T. Zehnder, "On the method of caustics: an exact analysis based on geometrical optics," J. Elasticity 15, 347–367 (1985).
14. M. L. Williams, "On the stress distribution at the base of a stationary crack," J. Appl. Mechan. 24, 109–114 (1957).
15. R. Narasimhan and A. J. Rosakis, "Finite element analysis of small scale yielding near a stationary crack under plane stress," J. Mechan. Phys. Solids 36, 77–117 (1988).
16. R. Narasimhan, A. J. Rosakis, and J. F. Hall, "A finite element study of stable crack growth under plane stress conditions: Part II—influence of hardening," J. Appl. Mechan. 109, 846–853 (1987).
17. A. T. Zehnder, "Dynamic fracture initiation and propagation in metals: experimental results and techniques," Ph.D. thesis, Caltech (1987).
18. R. Narasimhan and A. J. Rosakis, "Three dimensional effects near a crack tip in a ductile three point bend specimen part I: numerical analysis," Caltech Rept. SM88-6, submitted to J. Appl. Mechan.
19. A. T. Zehnder and A. J. Rosakis, "Three dimensional effects near a crack tip in a ductile three point bend specimen part II: experiments with caustics and interferometry," Caltech Rept. SM88-7, submitted to J. Appl. Mechan.
20. T. Nakamura, C. F. Shih, and L. B. Freund, "Analysis of a dynamically loaded three point bend ductile fracture specimen," Eng. Fracture Mechan. 25, 323-339 (1986).
21. J. A. Joyce and E. M. Hackett, "An advanced procedure for J-R curve testing in the drop weight tower," to be published in ASTM STP 995 *Nonlinear Fracture Mechanics*, Proc. Third Int. Symposium on Nonlinear Fracture Mechanics (Knoxville, Tenn., Oct. 6–8, 1986).
22. C. F. Shih, B. Moran, and T. Nakamura, "Energy release rate along a three-dimensional crack front in a thermally stressed body," Int. J. Fracture 30, 79–102 (1986).
23. A. J. Rosakis, A. T. Zehnder, and S. Krishnaswamy, "Dynamic measurement of the J integral in ductile metals: comparison of experimental and numerical techniques," Caltech Rept. SM88-8, scheduled for publication in Int. J. Fracture (1989).

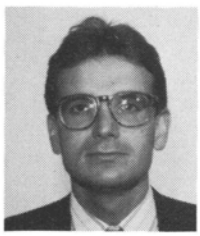

Ares J. Rosakis is an associate professor of aeronautics and applied mechanics at the California Institute of Technology. In 1978 he received a BA degree in engineering science from Oxford University. He obtained his masters and Ph.D. degrees in the area of solid mechanics and structures from Brown University in 1980 and 1982, respectively. In 1985 he was named Presidential Young Investigator by the National Science Foundation. His research work concentrates in the areas of nonlinear fracture, dynamic fracture mechanics, and plasticity.

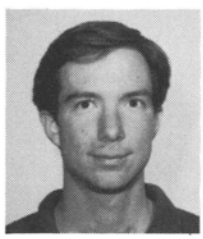

Alan Zehnder is an assistant professor in the Department of Theoretical and Applied Mechanics at Cornell University. He received his BS in mechanical engineering in 1982 at the University of California at Berkeley and his M.S. in 1983 and Ph.D. in 1987 both from the California Institute of Technology, in mechanical engineering. Dr. Zehnder works in the areas of nonlinear and dynamic fracture mechanics and in optical methods for experimental mechanics.

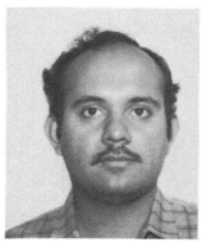

R. Narasimhan is an assistant professor in the Department of Mechanical Engineering at Indian Institute of Technology, Bombay. He received a bachelors degree in mechanical engineering from Indian Institute of Technology at Madras in 1982. He obtained his masters and Ph.D. degrees in applied Mechanics from the California Institute of Technology in 1983 and 1987, respectively. His research interests focus on numerical simulation of nonlinear and dynamic fracture processes and on dynamic plasticity.